Relationship between Tribology and Optics in Thin Films of Mechanically Oriented Nanocrystals

Liana Wong, Chunhua Hu, Ruthanne Paradise, Zina Zhu, Alexander Shtukenberg,* and Bart Kahr*

Department of Chemistry, New York University, 100 Washington Square East, Silver Center, Room 1001, New York, New York 10003, United States

S *Supporting Information*

ABSTRACT: Many crystalline dyes, when rubbed unidirectionally with cotton on glass slides, can be organized as thin films of highly aligned nanocrystals. Commonly, the linear birefringence and linear dichroism of these films resemble the optical properties of single crystals, indicating precisely oriented particles. Of 186 colored compounds, 122 showed sharp extinction and 50 were distinctly linearly dichroic. Of the latter 50 compounds, 88% were more optically dense when linearly polarized light was aligned with the rubbing axis. The mechanical properties of crystals that underlie the nonstatistical correlation between tribological processes and the direction of electron oscillations in absorption bands are discussed. The features that give rise to the orientation of dye crystallites naturally extend to colorless molecular crystals.

INTRODUCTION

Oriented thin films of organic chromophores[1] first showed their utility as light polarizers[2] and, more recently, have promised all manner of so-called photonic applications.[3−5] The earliest and arguably simplest way of making films of oriented dyes is by rubbing colored crystals along the length of a glass microscope slide. Brewster prepared the first artificially oriented dye films by rubbing grains of a crystalline anthraquinone in this way in 1846.[6] Subsequently, others have used mechanical forces to orient chromophores.[7] In the interim between Brewster and this report, a number of researchers have burnished dye films, especially pathologists working with histochemical stains. Zocher rubbed 160 dried drops of dye solutions, and with few exceptions, the most absorbing direction of the dichroic film was parallel to the rubbing direction.[8] Others have done likewise, observing a strong preference for positive linear dichroism (LD) that we define here as more absorbing in the rubbing direction.[9−11] Earlier researchers, if they tried to offer explanations, suggested that dye molecules, often elongated in the direction of the transition electric dipole moment corresponding to visible light absorption, are aligned individually and dragged in the rubbing direction in quite the same way polymers are brushed to anchor liquid crystals.[12−16] *This interpretation cannot be correct.* A dried droplet deposits crystallites, not individual molecules. Buffing orients crystals. How this works to produce positive LD 9 times out of 10 is not so easily reckoned. What is the relationship between tribology and photophysics? How does the action of crystal abrasion determine how the electrons in varied chromophoric films oscillate in polarized light?

In reinvestigating this body of work, we demonstrate the fidelity with which simple mechanical action can organize nanocrystals to give films with optical properties resembling single crystals. Moreover, we develop a crystal-chemical chain of events to explain the statistically improbable fact that 88% of dyes that form dichroic films show positive LD.

RESULTS

The compound that Brewster rubbed was called chrysammate (Gk. for *sand*) of potash.[6] It was originally prepared by treating the extract of aloes from Barbados with nitric acid and potassium carbonate.[17] The neutral compound, chrysammic acid (2,4,5,7-tetranitro-1,8-dihydroxyanthraquinone), can be prepared in the absence of aloe plants.[18] Treatment with K_2CO_3 yields the monopotassium salt. When several grains were rubbed with a cotton ball, or a piece of silk in Brewster's case, the resulting film, red in transmitted light and metallic in reflected light, was completely dichroic in the visible part of the spectrum (Figure 1a,b).

We have an extensive library of dyes well-distributed among textile dyes, histochemical stains, laser dyes, and fluorescent labels. We rubbed 186 randomly chosen dyes with cotton balls on untreated glass microscope slides with a back and forth motion along the long axis of the substrate. A few grains (∼5 mg) of dye particles taken directly from the supplier, or after recrystallization, were abraded in this way for approximately 10−60 s depending upon the rate at which they appeared to provide uniform films. Films showing nearly complete extinction between crossed polarizers were produced 122 times (68%) (Figure 2). (Seven compounds did not stick to glass and are excluded from these statistics.) Strikingly dichroic films were produced in a subset of these (50, 41%) (Figure 2). The optical properties of the rubbed films often resembled those of single crystals despite being composed of innumerable particles too small to be detected with a light microscope.
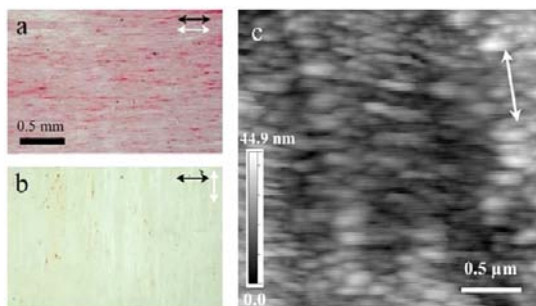
Figure 1. Chrysammate of potash (monopotassium salt of 2,4,5,7-tetranitro-1,8-dihydroxyanthraquinone) under polarized light (a) parallel and (b) perpendicular to the direction of rubbing. Black arrows indicate direction of applied light polarization, while white arrow indicates the rubbing direction. (c) AFM height image of the surface of the film.

However, the great majority of such dichroic films (44, 88%) absorbed more light when the polarizer was aligned with the long axis of the slides, the direction along which the finger was carried back and forth over the crystallites. A minority of dyes had greater optical density perpendicular to the rubbing direction (6 of 50). The probability of this outcome, assuming positive or negative LD equally likely, is $\sim 10^{-8}$. No intermediate optical density directions were observed.

The orientation distributions generated by Brewster's procedure were extremely tight as judged by imaging the linear birefringence (LB) and LD with the rotating polarizer method.[19,20] In this way, we can assay the most absorbing direction specified by some angle (θ), the most refracting direction (ϕ), as well as the quantities $|\sin(\delta)|$ and $\tanh(\varepsilon)$, where δ is linearly proportional to the LB, Δn, and the thickness (L), and $\tanh(\varepsilon)$ is related to the LD (see caption Figure 3). All four quantities are delivered for each camera pixel. The $\sim x = y$ dependence in Figure 3b shows the correlation of absorption and refraction anisotropy. Figure 3c,d shows that the magnitude of the LD and LB vary locally because of film thickness, but the range of orientations is extremely narrow. Small variances are indicated by the narrowness of the vertical streaks (Figure 3c,d). When one orientation parameter is plotted against the other we are left with a small cluster (Figure 3a); the organization of particles is extremely tight.

A variety of films were analyzed by atomic force microscopy (AFM). Chrysammate of potash (Figure 1c) revealed ellipsoidal particles ~ 100 nm in length with aspect ratios of $\sim 2:1$, closely packed, with their long axes uniformly perpendicular to the rubbing direction. Film thicknesses varied. They were typically less than 1 μm as judged by AFM, as well as scanning electron microscopy (SEM) and ellipsometry.

Closely packed ellipsoids with long axes perpendicular to the rubbing direction were seen for other compounds such as benzopurpurin in Figure 4. Researchers previously oriented crystalline semiconductors such as octathiophene or sexiphenyl using mechanical forces.[21-23] The microstructures of these films are virtually indistinguishable from those shown in Figures 1c and 4, indicating that certain features of the abrasion and orientation of nanocrystals by mechanical forces are quite general.

Microstructural analyses of nanocrystalline films prepared in this way must be treated cautiously. We observed that a number of films are not stable to immediate Ostwald ripening. The

instability of the films is evident in changing retardance immediately after rubbing (Figure 5b). This was confirmed by scanning electron micrographs (SEMs) in the case of disperse red 1 (DR1) that show elongated and remarkably similarly oriented crystals following post-abrasion growth (Figure 5a). The parallel outgrowth of the crystallites indicates how well their seeds were oriented.

■ DISCUSSION

How then are crystallites uniformly oriented by several passes of a finger so as to give films on glass with single-crystal-like extinction and positive LD? We know or surmised the following: (1) Molecular crystals of typical low symmetry (biaxial: triclinic, monoclinic, orthorhombic) have anisotropic elastic properties and will by necessity have anisotropic cleavage producing ellipsoidal particles on abrasion. (2) Like American football, ellipsoids will roll most effectively around their long axes. (3) Dye molecules tend to be extended and generally pack in elongated unit cells. (4) Assuming transition moments roughly parallel to the long axes of the molecules, the long unit cell axes will tend to be the most absorbing direction in transmitted, linearly polarized light. (5) According to the Bravais−Friedel−Donnay−Harker (BFDH) model[24-27] that aims to predict morphology on the basis of unit cell dimensions and symmetry, the lowest energy facets will be those that expose the highest reticular density, those perpendicular to the longest axis, taking account of submultiples of the interplanar spacing d_{hkl} arising from translational symmetry. In other words, the size of any face $\{hkl\}$ is inversely proportional to d_{hkl}. We then presume that faces exposed by abrasion will be the most stable. Thus, larger planes will be perpendicular to absorbing axes. Assuming 1−5 are obeyed with reasonable probability, then dye crystallites will align by rolling in the rubbing direction about some axis perpendicular to the direction of absorption, as shown schematically in Figure 4b.

Points 1−5 range from truisms to assumptions. They are evaluated here. Regarding (1), it is generally accepted that fracture of a crystal can occur by two mechanisms, breakage when the load overcomes the fracture strength and abrasion when the forces are concentrated at a small volume.[28] The energy required to produce abrasion fragments increases once the corners and edges are taken off.[29] However, researchers appear to have paid greater attention to modeling size distributions in mechanically disturbed crystals than in crystallographic directions exposed by abrasion.[30] Nevertheless, general ellipsoids should be the end point of the buffing processes described herein. Point (2) is an assumption based on a macroscopic analogy. We do know very much about how nanocrystallites tumble in response to shear. One can imagine that systems with perfect cleavage might subvert assumption (2). See forthcoming discussion. Point (3) is a consequence of a general knowledge of crystal structure. There are indeed positive correlations between the shapes of molecules and the shapes of unit cells. Point (4) is a corollary of (3), ignoring the complexity of chromophore coupling. We are presuming to say something about crystal optical properties on the basis of individual molecule orientations. A more proper description would consider the collective interactions among oscillators,[31] but the oriented gas interpretation is a good first approximation. Lastly, with respect to (5), we know the BFDH morphology disregards the anisotropy of forces in crystals and is wholly based on geometry.[32] Computationally efficient improvements to prediction of crystal morphology,
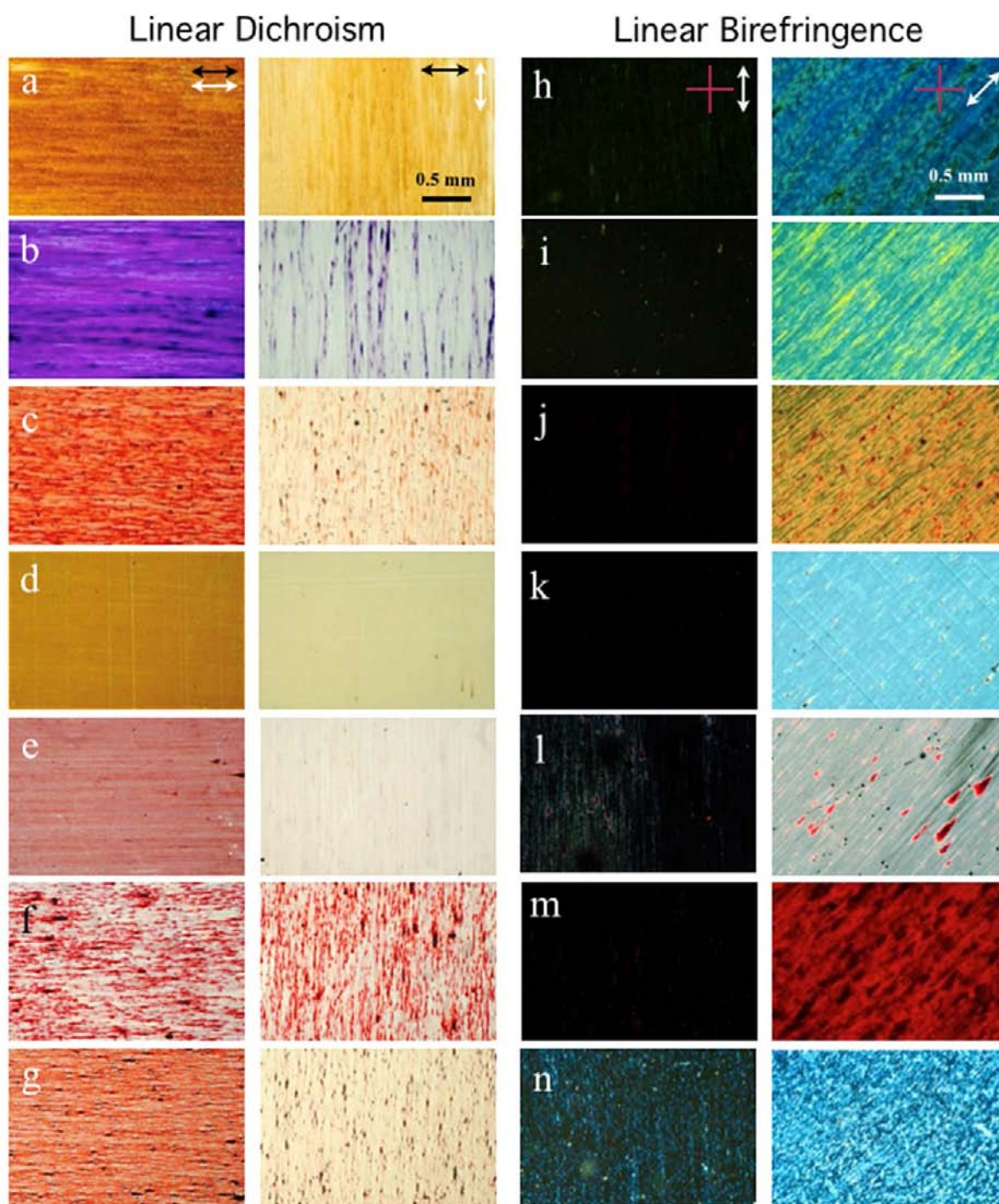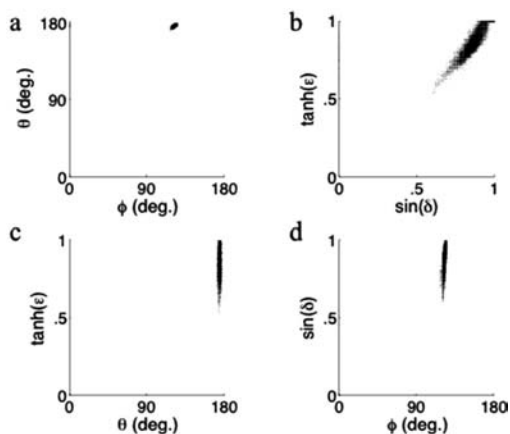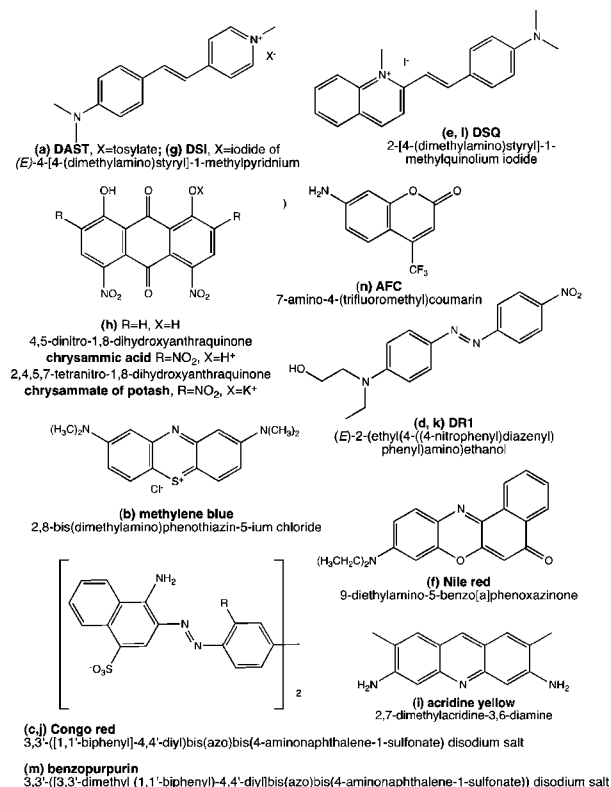
Figure 2. Various dye films in linearly polarized light (a−g) and between crossed polarizers (h−n). In (a−g) the left column, the direction of applied polarization (black arrows) is along the rubbing axis, while in the right column, the direction of applied polarization is perpendicular to the rubbing axis (white arrows). Pink crosses indicate the orientation of crossed polars. In (h−n), the left column shows the rubbing axis aligned with one of the polarizers, while the right column shows the film oriented ±45° between polarizers. (a) 4-[4-(Dimethylamino)styryl]-1-methylpyridnium tosylate (CAS: 24235-06-1); (b) methylene blue chloride (61-73-4); (c,j) Congo red (573-58-0); (d,k) disperse red 1 (2872-52-8); (e,l) 2-[4-(dimethylamino)styryl]-1-methylquinolium iodide (3915-61-5); (f) Nile red (7385-67-3); (g) 4-[4-(dimethylamino)styryl]-1-methylpyridnium iodide (68-971-03-9); (h) 4,5-dinitro-1,8-dihydroxyanthraquinone (81-55-0); (i) acridine yellow (92-26-2); (m) benzopurpurin (992-59-6); (n) 7-amino-4-(trifluoromethyl)coumarin (53518-15-3).

some applied to dye crystals, have been implemented,[33] but it is not clear to what extent such models, or any of the standard strategies (Hartman−Perdok theory,[34] equilibrium morphologies based on surface energies, or growth morphologies based on attachment energies[35]), apply to abrasion morphologies. Methods based on force fields must first be parametrized accurately, especially the partial charges that accompany ionic and charge transfer dyes. That said, the BFDH model has served crystallographers for generations as a rough prediction of habit. Few would deny that it contains a germ of truth, but it is by no means a law of nature.
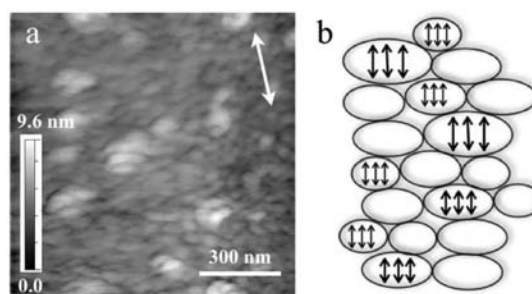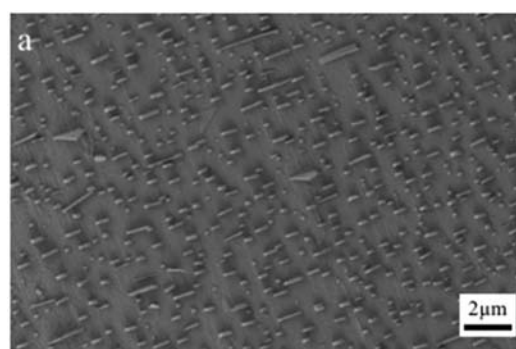
Scheme 1. Letters Refer to Figure 2

(a) DAST, X=tosylate; (g) DSI, X=iodide of
(E)-4-[4-(dimethylamino)styryl]-1-methylpyridnium

(e, l) DSQ
2-[4-(dimethylamino)styryl]-1-methylquinolium iodide

(n) AFC
7-amino-4-(trifluoromethyl)coumarin

(h) R=H, X=H
4,5-dinitro-1,8-dihydroxyanthraquinone
chrysammic acid R=NO₂, X=H⁺
2,4,5,7-tetranitro-1,8-dihydroxyanthraquinone
chrysammate of potash, R=NO₂, X=K⁺

(d, k) DR1
(E)-2-(ethyl(4-((4-nitrophenyl)diazenyl)phenyl)amino)ethanol

(b) methylene blue
2,8-bis(dimethylamino)phenothiazin-5-ium chloride

(f) Nile red
9-diethylamino-5-benzo[a]phenoxazinone

(i) acridine yellow
2,7-dimethylacridine-3,6-diamine

(c,j) Congo red
3,3'-([1,1'-biphenyl]-4,4'-diyl)bis(azo)bis(4-aminonaphthalene-1-sulfonate) disodium salt

(m) benzopurpurin
3,3'-([3,3'-dimethyl (1,1'-biphenyl)-4,4'-diyl]bis(azo)bis(4-aminonaphthalene-1-sulfonate)) disodium salt

Figure 4. (a) AFM height image of benzopurpurin. (b) Schematic of ellipsoidal particles with the transition electric dipole moments of elongated molecules perpendicular to the long axes.

Figure 3. Plots of optical parameters for chrysammate of potash based on automated LB (λ = 630 nm) and LD (λ = 514 nm) imaging nm. For 10 000 camera pixels over an area of 25 μm^2: (a) $\tanh(\varepsilon)$ vs θ; (b) $\sin(\delta)$ vs ϕ; (c) $\tanh(\varepsilon)$ vs $\sin(\delta)$; (d) ϕ vs θ; $\sin(\delta)$ where δ = $2\pi\Delta nL/\lambda$, $\tanh(\varepsilon)$ = $(T_\parallel - T_\perp)/(T_\parallel + T_\perp)$ where T is the transmittances for orthogonal polarizations and L is the thickness.


Figure 5. (a) SEM image of DR1 after recrystallization. Elongated laths are primarily extended perpendicular to the direction of rubbing. (b) Retardance ($|\sin(\delta)|$ where δ = $2\pi\Delta nL/\lambda$) decreases over time, t, suggesting a restructuring of the film; t = 0 is about 20 s after rubbing ceased; λ = 514 nm.

What follows is an evaluation of these ideas for particular substances. We reiterate that we are not aiming for the most precise description of any one system but rather to develop a framework to explain the fact that the most absorbing direction can be predicted 88% of the time without *any* knowledge of crystal or molecular structure.

Brewster's chrysammate of potash, the compound that was the progenitor of the work herein, was recrystallized from water, methanol, and ethanol as fine needles and thin, brittle plates, neither of which were suited for in-house X-ray crystal structure determination. Therefore, we cannot connect the shapes of the particles and optical properties of the films with structure in this case. We nevertheless were able to obtain a single-crystal structure of 2,4,5,7-tetranitro-1,8-dihydroxyanthraquinone K⁺18-crown-6·DMSO (see Supporting Information). Unfortunately, this compound did not make an oriented film. Nevertheless, we are not hidebound by the historical chrysammate.

DR1 and Nile red (NR) well illustrate the aforementioned hypotheses. DR1 crystallizes in the space group $P\bar{1}$, Z = 4.[36] Even though there are two independent molecules in the unit cell, the photophysics of this crystal is readily interpretable because both transition electric dipole moments of the molecules are roughly parallel to one another and roughly parallel to the longest axis of the unit cell: a = 7.540(1) Å, b = 11.366(1) Å, c = 19.358(3) Å, α = 83.58(2)°, β = 83.77(2)°, γ = 73.81(1)°. (The structures of commercial samples or recrystallized dyes used in our experiments were always confirmed by powder X-ray diffraction to ensure faithful

comparisons with structures in the literature). The BFDH morphology, a rough prediction of the shape of the abraded particle, is illustrated in Figure 6a. Indeed, the absorbing direction is roughly perpendicular to the long axis of the particle.
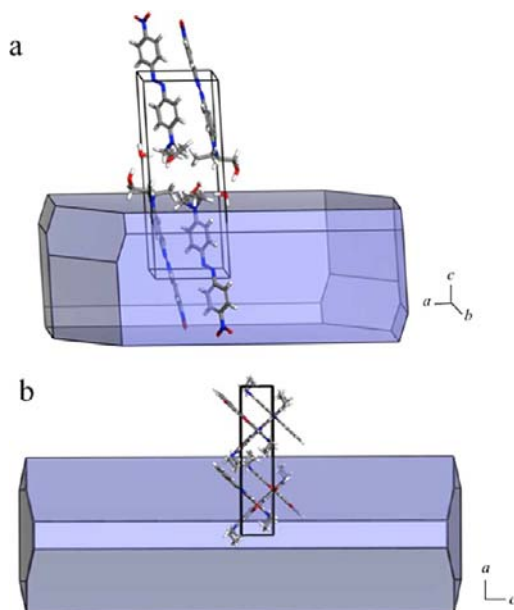
Figure 6. Predicted BFDH morphology of DR1 (a) and NR (b) shown with the contents of the unit cells. Molecules elongated along the long axis of the unit cell are perpendicular to the long axis of the crystallite in DR1, which absorbs much more strongly along the rubbing direction. In NR, the molecules cross each other and lie at some angle to the long axis of the crystallite. As we would expect, NR is less dichroic but absorbs slightly more light in the rubbing direction.

NR is a commonly used solvatochromic indicator.[37] Its structure has not been previously reported. NR was recrystallized from ethanol in the orthorhombic space group $Pna2_1$: a = 22.808(7) Å, b = 27.255(8) Å, c = 4.914(1) Å. The BFDH morphology for NR crystals predicts elongated particles (Figure 6b). However, NR molecules make a zigzag orientation with respect to the [011] direction. As such, in the absence of strong exciton coupling, we would expect a weak, but positive LD as in Figure 2f. Indeed, the dichroic ratios ($A_{\parallel}/A_{\perp}$) for films of DR1 and NR are 3.1 and 1.2, respectively.

2-[4-(Dimethylamino)styryl]-1-methylquinolium iodide (DSQ) also shows strong, positive LD (Figure 2e,l). DSQ crystallizes from alcohols as {001} plates (Figure 7a) that cleave consistently along two directions (Figure 7b) when plates fracture under mild pressure.[38] X-ray diffraction reveals these two cleavage planes as {001} and {010} (Figure 7d). This results in rods elongated along the a axis. The absorption should be most pronounced along c, again along the shorter axis of ellipsoids that would be generated by abrasion. In this instance, as seen in Figure 7c, the BFDH morphology is not terribly discriminating and is a poor approximation of the growth morphology (Figure 7a). Fracture nevertheless conspires to yield the common observation of positive LD for buffed films. Addition of water gives more isometric habits resembling the BFDH prediction. Of course, dependence of habit on growth conditions cannot be captured in the BFDH model which relies only on unit cell dimensions.
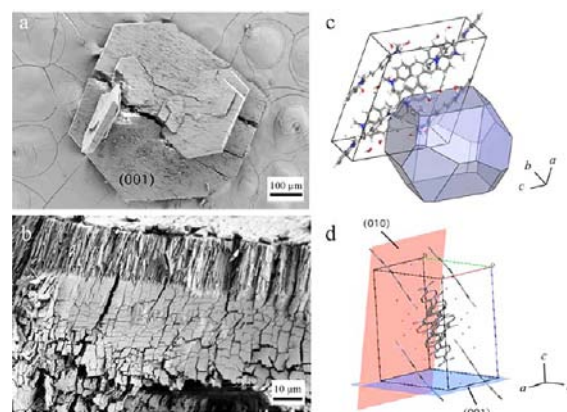
Figure 7. (a) DSQ plates after light pressure was applied with a razor blade (b), imaged with a SEM. Cleavage occurs parallel to {001} and {010} illustrated by the cracks. (c) Predicted BFDH morphology for DSQ. (d) These cleavage planes result in rods elongated along a. Crystal data: a = 20.8997(4) Å; b = 10.5941(2) Å; c = 18.4020(4) Å, β = 113.047(1)°, space group $C2/c$. Hydrogen atoms removed for clarity.

As indicated, 12% of dichroic films absorb light more strongly in the direction perpendicular to the rubbing axis. An analysis of the crystal structure should suggest a reason why they behave contrary to the established "rule". Exceptions can arise by two mechanisms. The transition electric dipole moment may lie along the long axis of the abraded particle, or the particles may align with their long axes in the direction of the applied force. 2,2′-Azidobis(3-ethylbenzthiazoline-6-sulfonic acid) diammonium salt (AES) absorbs more light when the input polarization is *perpendicular* to the rubbing direction. This may be explained through an analysis of its crystal structure.[39] Like DSQ, AES is ionic. The dye molecules and corresponding transition moment are aligned parallel to the long axis of the unit cell, as with most dyes. Similarly, the BFDH predicted morphology shows the long axis of the unit cell perpendicular to the long axis of the crystal (Figure 8). However, planes of ions or ionic groups, NH_4^+ and $-SO_3^-$, respectively, lie perpendicular to the long axis, strengthening the crystal in this direction. Therefore, the crystal will be more likely to cleave *parallel* to the elongated dye molecules, the green planes in Figure 8, resulting in greater absorption perpendicular to the rubbing direction.

7-Amino-4-(trifluoromethyl)coumarin (AFC) particles in Figure 9b are elongated *along* the rubbing direction. This is a consequence of plank-like morphologies (Figure 9a) that result from perfect (001) and (1$\bar{1}$1) cleavage. These particles do not roll but are rather dragged in the direction of the shearing force (surf boards align with the current).[40] We would thus anticipate negative LD on the basis of this fact alone. However, for "short" dye molecules, the BFDH morphology is not very predictive (Figure 9d) of optical properties.[41] In the case of AFC, hydrogen bonding is the strongest intermolecular force, occurring between the carbonyl and amine groups in the (1$\bar{1}$1) plane. We would thus envisage cleavage along—not across as the BFDH model suggests—this plane, as well as between the {001} trifluoromethyl groups (Figure 9c). Indeed, we established by X-ray diffraction that these are the principle cleavage planes. The consistent valence force field (CVFF),[42] likely to improve the predicted morphology for this neutral dye, gave an equilibrium morphology based on computed surface energies that increased the importance of {001} and {1$\bar{1}$1}

12249

dx.doi.org/10.1021/ja304799a | *J. Am. Chem. Soc.* 2012, 134, 12245−12251
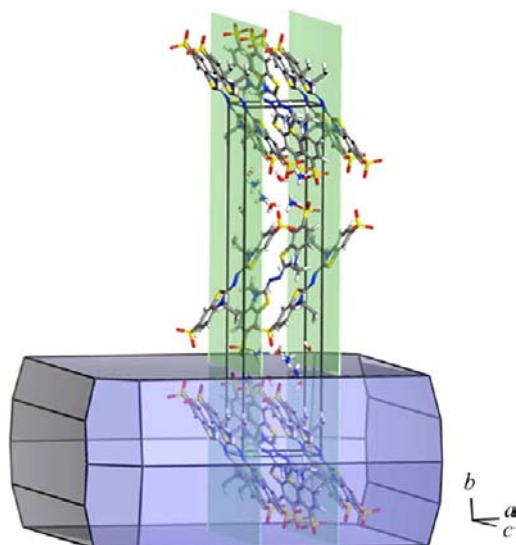
Figure 8. Predicted BFDH morphology and unit cell of AES. As we would expect, molecules are elongated perpendicular to the long axis of the crystal. However, green planes indicate expected cleavage—the crystal will tend to avoid breaking along planes (010) containing the ionic bonds. This results in ellipsoidal crystallites with the transition electric dipole moment *parallel* to the football's long axis. Crystal data: $a = 8.707(1)$ Å, $b = 36.843(7)$ Å, $c = 8.222(1)$ Å, $\beta = 97.18(3)°$, space group $P2_1/c$.

Figure 9. (a) SEM image of AFC crystallized from a mixture of ethanol and chloroform (1:2) after light pressure was applied with a razor blade. Perfect cleavage is seen along (001) or $(1\bar{1}1)$. (b) AFM height image of AFC after rubbing along the axis indicated by a doubled headed white arrow. (c) Predicted cleavage along (001) and $(1\bar{1}1)$, which leaves the hydrogen bond intact. (d) Calculated BFDH morphology of AFC with unit cell and direction of electronic transition dipole moment indicated by red double-headed arrow. Neither the (001) nor the $(1\bar{1}1)$ face is expressed. (e) Calculated equilibrium morphology using the CVFF force field. Both (001) and $(1\bar{1}1)$ are present: $a = 5.190(3)$ Å, $b = 6.882(4)$ Å, $c = 14.165(4)$ Å, $\alpha = 82.72(6)°$, $\beta = 85.54(6)°$, $\gamma = 72.67(4)°$, space group $P\bar{1}$.

faces. When the transition electric dipole moment of the AFC unit cell was calculated and compared to the computed equilibrium morphology, the absorption was predicted to lie along the long axis of the particle (Figure 9e). Here, two contrary behaviors conspire to mimic what happens most commonly with dyes.
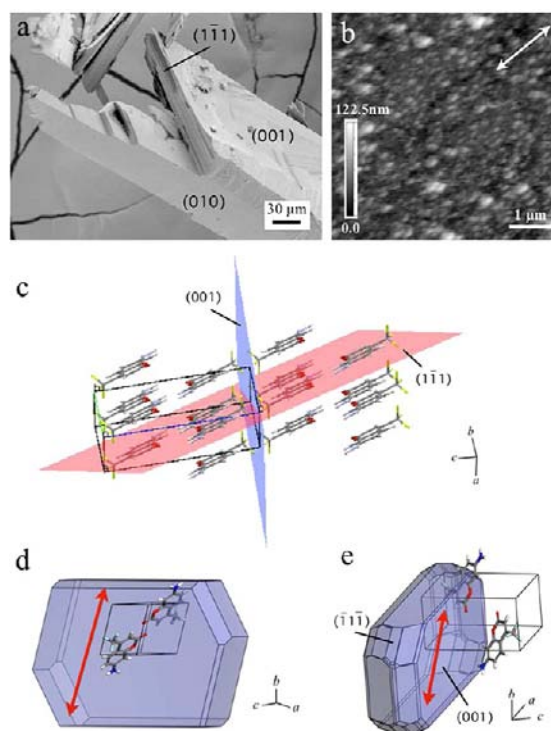
The principles that govern the mechanical alignment of nanocrystals naturally may be applied to colorless compounds. To illustrate this, we chose 4-hydroxybenzoic acid, a compound on hand with established cleavage[43] that makes films easily. Figure 10 shows the sharp extinction after rubbing for <60 s.
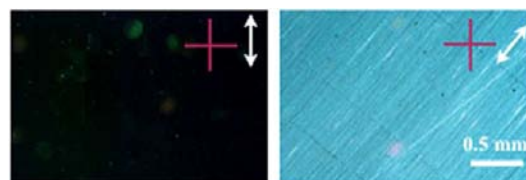
■ **SUMMARY**

An experimental historical reinvestigation of the first example of artificially produced dichroism was the starting point for the work described herein.[6] A consideration of what Brewster had achieved suggested a reinterpretation of the literature on the mechanical orientation of histochemical stains[8−11] among other compounds.[17,18] The strong correlation between the action of rubbing and the photophysical behavior of the resulting films— striking for their single-crystal-like qualities—indicated that there must be an interpretation embedded in the characteristics of dye crystals. Through microstructural analysis of films of organized nanoparticles, in conjunction with known crystal structures of dyes, we explained why the great majority of crystallites are oriented so as to absorb light in the rubbing direction. Recently, researchers have attempted to use magnetic fields,[44] electric fields,[45] sols,[46] polymers,[47] and epitaxial growth[48] to orient organic nanocrystals. None of these methods are as easy or as general as that described herein.

■ **EXPERIMENTAL SECTION**

Rotating Polarizer Method. Linear optical properties were measured by the rotating polarizer method using a prototype of the Metripol microscope.[19] The optical train for imaging linear retardance

Figure 10. Birefringence of a 4-hydroxybenzoic acid rubbed film. Left: extinction position. Right: orientation between crossed polarizers (pink cross). White arrow indicates rubbing axis. Crystal data: $a = 18.508(7)$ Å, $b = 5.228(2)$ Å, $c = 6.342(3)$ Å, $\beta = 93.22(3)°$, space group $P2_1/a$.

consists of a light source (one of four LEDs: 457, 514, 588, and 630 nm), rotating polarizer, sample, objective, $\lambda/4$ waveplate, and followed by a polarizer aligned at 45° relative to the fast axis of the $\lambda/4$ wave plate. The theory is described elsewhere.[16]

Atomic Force Microscopy. Height and deflection images were recorded with an MFP-3D-SA system (Asylum Research) and with a Veeco Multimode system. Measurements were performed in contact mode at a deflection of −2.0 V.

Scanning Electron Microscopy. The samples were mounted on conductive carbon tape, adhered on aluminum holders, and then coated with 5 nm of gold. The images were recorded with a MERLIN field-emission scanning electron microscope (Carl Zeiss) using a standard Everhart−Thornley type detector at an acceleration voltage of 1−3 kV.

X-ray Diffraction. Phase confirmation and crystal indexing was performed with a Bruker AXS D8 DISCOVER GADDS micro-diffractometer equipped with a VÅNTEC-2000 two-dimensional detector and a 0.5 mm MONOCAP collimator (Cu Kα radiation). Single-crystal structures were determined with a Bruker AXS SMART APEXII single-crystal diffractometer (Mo Kα radiation).

Computations. BFDH and equilibrium morphologies were calculated and plotted with Accelrys Materials Studio version 4.2. Transition moments for crystals were calculated with Gaussian09, version B.01 (see Supporting Information for full citation).

■ ASSOCIATED CONTENT

ⓢ Supporting Information

Crystal structure for 2,4,5,7-tetranitro-1,8-dihydroxyanthrraqui-none K⁺18-crown-6·DMSO and NR, as well as full Gaussian citation. This material is available free of charge via the Internet at http://pubs.acs.org.

■ AUTHOR INFORMATION

Corresponding Author
bart.kahr@nyu.edu; shtukenberg@mail.ru
Notes
The authors declare no competing financial interest.

■ ACKNOWLEDGMENTS

■ REFERENCES

(1) Michl, J.; Thulstrup, E. W. *Spectroscopy with Polarized Light*; Wiley-VCH: Weinheim, Germany, 1995.

(2) Land, E. H.; West, C. D. *Colloid Chemistry*; Alexander, J., Ed.; Van Nostrand Reinhold: New York, 1946; Vol. 6, pp 160−190.

(3) Patra, A.; Chadaluri, Ch. G.; Radhakrishnan, T. P. *Nanoscale* **2012**, *4*, 343−359.

(4) Würthner, F., Ed. *Supramolecular Dye Chemistry*; Springer: Berlin, 2005.

(5) Horie, K.; Ushiki, H.; Winnik, F. M. *Molecular Photonics: Fundamental and Practical Aspects*; Wiley-VCH: Weinheim, Germany, 2000.

(6) Brewster, D. *Philos. Mag.* **1846**, *29*, 331−332.

(7) Seherr-Thoss, M. *Ann. Phys.* **1879**, *242*, 270−287.

(8) (a) Zocher, H. *Naturwissenschaften* **1925**, *50*, 1015−1021. (b) Zocher, H.; Jacoby, O. *Kolloidchem. Beih.* **1927**, *24*, 365−417.

(9) Goldstein, D. J. *J. Microsc.* **1969**, *89*, 19−36.

(10) Goldstein, D. J.; Horobin, R. W. *Histochem. J.* **1974**, *6*, 175−184.

(11) Howie, A. J.; Brewer, D. B. *Micron* **2009**, *40*, 285−301.

(12) Mauguin, C. *Bull. Soc. Fr. Min.* **1911**, *34*, 71−76.

(13) Berreman, D. W. *Phys. Rev. Lett.* **1972**, *28*, 1683−1686.

(14) Stöhr, J.; Samant, M. G.; Cossy-Favre, A.; Diaz, J.; Momoi, Y.; Odahara, S.; Nagata, T. *Macromolecules* **1998**, *31*, 1942−1948.

(15) Damman, P.; Coppée, S.; Geskin, V. M.; Lazzaroni, R. *J. Am. Chem. Soc.* **2002**, *124*, 15166−15167.

(16) Liu, S.; Wang, W. M.; Briseno, A. L.; Mannsfeld, S. C. B.; Bao, Z. *Adv. Mater.* **2009**, *21*, 1217−1232.

(17) Gmelin, L. *Handbook of Chemistry*; Watts, H. (translated); Cavendish Society: London, 1858; Vol. *XII*, pp 1−7.

(18) Teich, L.; Daub, K. S.; Krügel, V.; Nissler, L.; Gebhardt, R.; Eger, K. *Bioorg. Med. Chem.* **2004**, *12*, 5961−5971.

(19) Glazer, A. M.; Lewis, J. G.; Kaminsky, W. *Proc. R. Soc. London A* **1996**, *452*, 2751−2765.

(20) Kaminsky, W.; Claborn, K.; Kahr, B. *Chem. Soc. Rev.* **2004**, *33*, 514−525.

(21) Videlot, C.; Grayer, V.; Ackermann, J.; El Kassmi, A.; Fichou, D. *Synth. Met.* **2003**, *139*, 115−122.

(22) Chen, X. L.; Lovinger, A. J.; Bao, Z.; Sapjeta, J. *Chem. Mater.* **2001**, *13*, 1341−1348.

(23) Hu, W.-S.; Lin, Y.-F.; Tao, Y.-T.; Hsu, Y.-J.; Wei, D.-H. *Macromolecules* **2005**, *38*, 9617−9624.

(24) Bravais, A. I *Études Cristallographiques*; Gauthier-Villars: Paris, 1866.

(25) Friedel, G. *Bull. Soc. Fr. Min.* **1907**, *30*, 326−455.

(26) Donnay, J. D. H.; Harker, D. *Am. Mineral.* **1937**, *22*, 463−468.

(27) Hartman, P. *Can. Mineral.* **1978**, *16*, 387−391.

(28) Mazzarotta, B. *Chem. Eng. Sci.* **1992**, *47*, 3105−3111.

(29) Nienow, A. W.; Conti, R. *Chem. Eng. Sci.* **1978**, *33*, 1077−1086.

(30) Biscans, B.; Guiraud, P.; Laguérie, C.; Massarelli, A.; Mazzarotta, B. *Chem. Eng. J.* **1996**, *63*, 85−91.

(31) Tristani-Kendra, M.; Eckhardt, C. J.; Bernstein, J.; Goldstein, E. *Chem. Phys. Lett.* **1983**, *98*, 57−61.

(32) Prywer, J. *J. Cryst. Growth* **2004**, *270*, 699−710.

(33) Deij, M. A.; Meekes, H.; Vlieg, E. *Cryst. Growth Des.* **2007**, *7*, 1949−1957.

(34) Woensdregt, C. F. *Faraday Discuss.* **1993**, *95*, 97−107.

(35) Coombes, D. S.; Catlow, C. R. A.; Gale, J. D.; Rohl, A. L.; Price, S. L. *Cryst. Growth Des.* **2005**, *5*, 879−885.

(36) Lacroix, P. G.; Malfant, I.; Iftime, G.; Razus, A. C.; Nakatani, K.; Delaire, J. A. *Chem.—Eur. J.* **2000**, *6*, 2599−2608.

(37) Murugan, N. A.; Rinkevicius, Z.; Ågren, H. *Int. J. Quantum Chem.* **2011**, *111*, 1521−1530.

(38) Chantrapromma, S.; Kobkeatthawin, T.; Chanawanno, K.; Karalai, C.; Fun, H.-K. *Acta Crystallogr., Sect. E* **2008**, *64*, o876−o877.

(39) Mousty, C.; Therias, S.; Aboab, B.; Molinie, P.; Queignec, M.; Leone, P.; Rossignol, C.; Palvadeau, P. *New J. Chem.* **1997**, *21*, 1321−1330.

(40) This distinction can be made as we have with dried pasta. Short lengths of spaghetti roll while short lengths of linguini drag. Perpendicular and parallel orientations result, respectively, when brushed with paper.

(41) Selladurai, S.; Subramanian, K. *Acta Crystallogr., Sect. C* **1992**, *48*, 281−283.

(42) Dauber-Osguthorpe, P.; Roberts, V. A.; Osguthorpe, D. J.; Wolff, J.; Genest, M.; Hagler, A. T. *Proteins: Struct., Funct., Genet.* **1988**, *4*, 31−47.

(43) Reddy, C. M.; Krishna, G. R.; Ghosh, S. *CrystEngComm* **2010**, *12*, 2296−2314.

(44) Kaneko, Y.; Shimada, S.; Fukuda, T.; Kimura, T.; Yokoi, H.; Matsuda, H.; Onodera, T.; Kasai, H.; Okada, S.; Oikawa, H.; Nakanishi, H. *Adv. Mater.* **2005**, *17*, 160−163.

(45) Macchi, R.; Cariati, E.; Marinotto, D.; Tordin, E.; Ugo, R.; Santoro, G.; Ubaldi, M. C.; Pietralunga, S. M.; Mattei, G. *J. Mater. Chem.* **2011**, *21*, 9778−9783.

(46) Takahashi, M.; Figus, C.; Kichob, T.; Enzo, S.; Casula, M.; Valentini, M.; Innocenzi, P. *Adv. Mater.* **2009**, *21*, 1732−1736.

(47) Denisyuk, I. Yu.; Burunkova, J. E. *Mol. Cryst. Liq. Cryst.* **2007**, *467*, 213−226.

(48) Yanagi, H.; Shibutani, T. *Thin Solid Films* **2003**, *438*, 33−38.